Lattice instability and superconductivity in electron doped (3, 3) carbon nanotubes

2009 J. Phys.: Condens. Matter 21 084206

(http://iopscience.iop.org/0953-8984/21/8/084206)

IOP PUBLISHING JOURNAL OF PHYSICS: CONDENSED MATTER

J. Phys.: Condens. Matter **21** (2009) 084206 (7pp) doi:10.1088/0953-8984/21/8/084206

Lattice instability and superconductivity in electron doped (3, 3) carbon nanotubes

K-P Bohnen[1], **R Heid**[1] **and C T Chan**[2]

[1] Forschungszentrum Karlsruhe, Institut für Festkörperphysik, POB 3640, D-76021 Karlsruhe, Germany

[2] Department of Physics and Institute for Nano Science and Technology, Hong Kong University of Science and Technology, Clear Water Bay, Hong Kong, People's Republic of China

Received 18 July 2008
Published 30 January 2009
Online at stacks.iop.org/JPhysCM/21/084206

Abstract

We investigated the effect of electron doping on the phonon dispersion and electron–phonon coupling of a small diameter (3, 3) carbon nanotube using first principles density functional perturbation theory. Electron doping increases the number of nesting features in the electronic band structure, which is reflected in a wealth of phonon anomalies. We found that the overall electron–phonon coupling is substantially enhanced with respect to the pristine tube, which improves superconductivity. At the same time, the intrinsic Peierls instability remains similar, but the Peierls temperature still remains larger than the superconducting transition temperature.

(Some figures in this article are in colour only in the electronic version)

1. Introduction

Modern *ab initio* methods have opened the way to study geometric structure, band structure, lattice dynamics, and even electron–phonon interactions for complex systems in great detail. Today it is possible to investigate the influence of structural changes, doping with different kinds of atom, and external fields on electronic and phononic properties without relying on experimental input. This allows us to elucidate the role of individual components in multi-component systems with the option to develop materials with special functionalities. One field in which these features are of great importance is the area of carbon nanotubes [1], which have attracted a lot of attention from scientists and engineers. One key reason for their importance for both science and technology is the small diameter of these tubes, which is typically of the order of a nanometer for single wall carbon nanotubes (SWNTs). A small diameter implies that a nanotube is an extremely sharp needle, and hence an excellent field emitter. It is also the narrowest conducting wire, and can transport electrons in a ballistic manner. These desirable properties depend on the good conductivity of the nanotubes. However, the phenomenon of Peierls transition dictates that a truly one dimensional (1D) conductor will spontaneously open a gap at $T = 0$ K due to strong electron–phonon interaction, which is a consequence of the diverging susceptibility at 1D. Since real systems are never truly 1D, there is a finite Peierls transition temperature T_D below which the tubes undergo a lattice distortion and become semiconductors. For temperatures higher than T_D, the electron–phonon coupling effect will manifest as a dip in the phonon dispersion, which is the Kohn anomaly. As the temperature is lowered towards T_D, the phonon frequency at the Kohn anomaly will decrease continuously towards zero frequency and the mode will eventually become 'soft', signaling a transition to a lattice-distorted structure with a lower energy, and the equilibrium atomic coordinates in the distorted state will be given by higher-order terms of the Hamiltonian. The phenomenon of Peierls transition and soft phonons is thus of great importance for the physical properties of an extremely narrow conductor that approaches the limit of a 1D system.

For SWNTs, the smallest diameter tubes that can be made in a controllable manner and in a substantial quantity are probably the 0.4 nm diameter tubes that are fabricated using a zeolite template method [2]. It is difficult to produce nanotubes of such a small diameter, since the ultra-small diameter implies a large curvature and strain and these small diameter tubes are not favorable in energy. However, recent advances in fabrication techniques enable fabrication of these tubes inside the confined channels of zeolite AlPO4-5 single crystals, and inside the zeolite channels only SWNTs of 0.4 nm can form. There are three types of tube ((3, 3), (4, 2) and (5, 0)) of approximately 0.4 nm in diameter, and they are all found inside the zeolite channels. The (3, 3) and (5, 0) tubes are metallic

according to standard band structure calculations [3, 4], and these ultra-small tubes are as close to a 1D conductor that we can get and are thus interesting systems to study electron–phonon (el–ph) interactions. There have already been very careful calculations on lattice dynamics and el–ph interactions for these tubes, and for the (3, 3) tube it was found that a phonon branch becomes soft at $q = 2k_F$ at about room temperature [5, 6]. In the present paper, we examine the lattice dynamics and el–ph interactions when the (3, 3) tube is doped with electrons. We will see that electron doping shifts the Fermi level to a higher energy and the changes in the phonon dispersion and el–ph interactions are substantial.

Superconducting behavior has been reported [7] in these ultra-small nanotubes embedded in zeolite hosts. The origin of the superconductivity is still under investigation. As the superconductivity and Peierls transition both derive from the electron–phonon mechanism, they are competing against each other. There is evidence from previous studies that the strong curvature of graphitic nanostructures, including small diameter nanotubes, can enhance electron–phonon interactions, giving the possibility of superconductivity in a pure carbon system [8]. However, a smaller radius also implies a higher Peierls temperature T_D and therefore it is not clear which phenomenon will prevail. For both (5, 0) and (3, 3) nanotubes, first principles density functional calculations for isolated tubes found that T_D should be significantly higher than the reported T_c of about 15 K [5, 6]. For isolated pristine ultra-small radius tubes, Peierls instability should pre-empt superconductivity. We note that the theory papers consider an array of tubes with tube–tube distance large enough so that the results correspond to truly quasi-1D non-interacting systems, while in the experiment the tubes are always residing inside the zeolite channels. It is possible that the lateral coupling with the host matrix reduces the 1D character of the system and thus suppresses the Peierls instability. In addition, the system is chemically complex and there will be some electron transfer between the tubes and the host and other impurities, and thus the situation of the experiment corresponds to a doped tube, rather than a pristine tube.

In this paper, we will investigate whether doping the (3, 3) nanotube with electrons can promote superconductivity. We are motivated by the following considerations. It is known that graphite intercalated compounds and alkali intercalated C_{60} have superconducting phases [9], and the superconductivity comes from el–ph interaction. It is thus tempting to investigate whether electron doped tubes can be superconducting. In addition, previous calculations [10] found that adding excess electrons to the (3, 3) tube can increase the electronic density of states, which can potentially enhance T_c. Electron doping can be achieved by intercalating Li to the nanotube zeolite complex. The intercalated Li will fill up the space between the tubes and the host. The intercalation will most probably reduce the 1D character and suppress the Peierls transition much more efficiently. This points to the possibility that Li intercalated nanotube–zeolite complex should exhibit superconductivity at a higher temperature than the pristine nanotube–zeolite complex.

We will see that the results of the present calculation show that upon electron doping the T_D remains more or less the same as for an isolated tube (although the details at the microscopic level are rather different), but the T_c is enhanced significantly.

2. Method of calculation

In this paper, we employ the density functional perturbation theory (DFPT) [11] to study the lattice dynamics and electron–phonon interaction of (3, 3) nanotubes in the presence of electron doping. Our DFPT scheme is implemented in a 'mixed-basis' pseudopotential code [12, 13], which uses both plane waves and local orbitals to expand the electronic wavefunction and norm-conserving pseudopotentials to describe the electron–core interaction. The plane waves cut-off is set at 20 Ryd, augmented by localized 2s-and 2p-like functions. The mixed-basis DFPT code has been applied successfully to describe the phonon dispersion, electron–phonon coupling and superconductivity properties of many systems.

The DFPT has the advantage that it gives the phonon dispersion at arbitrary phonon wavevectors. In contrast, calculating phonon frequencies by extracting force constants from supercell calculations is limited to phonons with wavelengths that are compatible with the supercell. The DFPT is the method of choice for studying the Peierls instability since phonon anomalies can occur at phonon wavevectors that may be incommensurate with the lattice.

Alternative methods, such as the tight-binding method [14] and zone-folding schemes [15], are less computationally demanding. These methods are very useful for nano-graphitic structures in general and for carbon nanotubes with diameters larger than one nanometer. However, for the 0.4 nm diameter nanotubes we are studying, the curvature effect is significant and that changes the band structure predicted from zone-folding. For example, the Fermi wavevector (k_F) is pinned at $2/3\ \Gamma X$ in the zone-folding scheme for any member of the (n, n) tube family, but the curvature effect actually pushes the k_F closer to the zone center, so that $k_F = 0.57\ \Gamma X$ for the pristine (3, 3) tube. The slope of the bands also changes near k_F. As we expect a nesting $q = 2k_F$ for the undoped tube, the curvature effect can have a significant effect on the phonon anomalies. Another complexity is that we are considering tubes that are doped with extra electrons. As the curvature effect also changes the slope of the bands from those of zone-folded results, electron doping will also introduce another level of unknown error if we employ zone-folding. Methods such as tight binding are fast, results are easy to interpret and additional parameters can be added at will, but strong curvature effects and electron doping probably will be too demanding for most tight-binding methods.

The nanotubes are arranged in a hexagonal array, with a nearest wall-to-wall distance of 10 Å. Such a large distance between the tubes minimizes inter-tube interactions, so that our results are relevant for describing an isolated tube. We use Gaussian broadening near the Fermi level. For structural relaxations, we used a Gaussian width of 0.2 eV. A set of smaller Gaussian widths is used for phonon calculations to provide various degree of sharpness in sampling the Fermi surface. For electron–phonon coupling calculations, we

Table 1. The nesting q-vectors in order of increasing magnitude and the Fermi points connected by them.

Nesting vector	$k_4 - k_3$	$k_3 - k_2$	$2k_4$	$2k_3$	$k_2 - k_1$	$k_2 + k_4$	$k_4 - k_1$	$2k_2$	$k_1 + k_3$	$2k_1$
Magnitude (π/a)	0.084	0.100	0.156	0.324	0.338	0.340	0.522	0.524	0.762	0.800

employed a k-point grid of 1024 points along (0, 0, k_z) in the Brillouin zone (BZ).

Electron doping is accomplished by adding one extra electron to the system, which has 12 carbon atoms in the primitive unit cell. A uniform neutralizing background is added to maintain charge neutrality. The advantage of this approach is that the unit cell remains the same and the symmetry of the system is preserved, so the computer cost can be manageable, and it also allows for an easier comparison with the pristine phonon results.

It is known that graphitic structures, such as graphite and fullerene crystals, can be intercalated with alkaline metals, and the electrons from the alkaline metals will be donated to the carbon. In many cases, the alkaline intercalated systems become metallic and many of them exhibit superconductivity. The family of compounds X_3C_{60} (where X is an alkali element) can reach a rather high superconducting temperature [9], and the high T_c can be correlated with the high density of states near E_F for these compounds. The change in the band structure of these materials can frequently be described by a rigid-band picture near the Fermi level, with extra states near the Fermi level being filled. The same situation was found for (3, 3) tubes. The electronic structure of the (3, 3) tube doped with Li was studied in detail previously [10], and the results showed that the rigid-band picture is a very good approximation near the Fermi level at least up to a high Li concentration of 8%. In other words, the Li donates its electron to the carbon, and the band structure of Li@(3, 3) near the Fermi level is basically that of filling up the bands of (3, 3) with extra electrons. Our electron doping results should be a reasonably good description for considering the effect of Li and alkali metal doping on the lattice dynamical properties of carbon nanotubes. Both theory and experiment found that the nanotube–zeolite complex can absorb a high atomic percentage of Li [16].

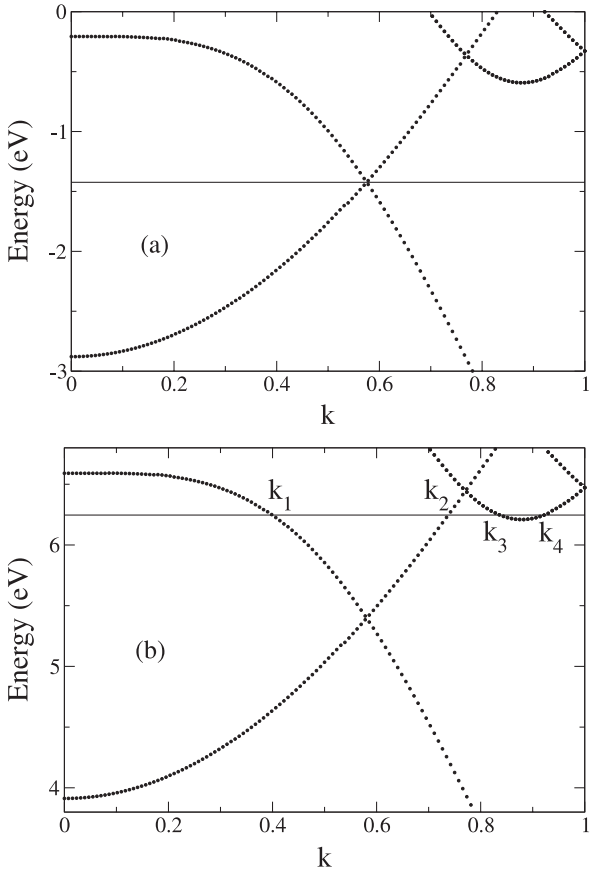

Figure 1. The band structure of (a) pristine (3, 3) and (b) doped (3, 3) tubes. The electron doped (3, 3) has one excess electron per 12 C atoms. We note that the Fermi level intersects the bands at four k points in the irreducible BZ. k is given in units of π/a.

3. Results

3.1. Electronic structure

Before we examine the phonon dispersion, we first take a look at the electronic band structure of the doped (3, 3) tube, and compare it with that of the pristine tube. The band structure of pristine (3, 3) is shown in figure 1(a), and that of electron doped (3, 3) with a doping of one additional electron per 12 C atoms is shown in figure 1(b). If we compare figure 1(b) with the band structure of Li doped (3, 3) with a nominal formula of C_{12}Li [10], we see that the bands near E_F are almost identical. From figure 1(b), we observe that the Fermi level intersects the bands at four k points in the irreducible BZ. These four points are labeled as k_1, k_2, k_3, and k_4, respectively. Their magnitudes are given by $k_1 = 0.400\ \pi/a$, $k_2 = 0.738\ \pi/a$, $k_3 = 0.838\ \pi/a$, $k_4 = 0.922\ \pi/a$.

For the pristine (3, 3) tube, the Fermi level is pinned at the crossing of the two π and π^* bands, one with a positive effective mass and the other with a negative mass. With excess electrons donated to the tube, the additional electrons will raise the Fermi level so that it will cut these two bands at different k vectors, with the smaller k_1 corresponding to that of the negative mass band, and a larger k_2 corresponding to the positive mass band. Adding more electrons will eventually push the Fermi level past a van Hove singularity as the valley due to another band starts filling up, and this contributes two additional Fermi points at k_3 and k_4. In the limit of zero doping, only k_1 and k_2 will cut the Fermi level and $k_1 = k_2$. Taking into account all nesting q-vectors that connect these k-points and only considering those such that the electronic bands have slopes with opposite signs on either side of the q-vector (which give diverging susceptibility in 1D systems), we can identify a set of nesting vectors that will cause strong el–ph coupling for the doped tube. These q-vectors are listed in table 1. Due to the proliferation of q-vectors in the doped case, we expect that the phonon anomalies will be much more complex than in the pristine (3, 3) tube, in which the only two nesting q-vectors are $k_2 - k_1 = 0$ and $2k_1 = 2k_2$.

3.2. Phonon dispersion

Phonon dispersions calculated by DFPT for the electron doped (3, 3) tube are shown in figure 2. Figures 2(a) and (b) are computed with two broadening widths of 0.2 and 0.025 eV. These Fermi surface smearings can be interpreted as corresponding to effective temperatures of approximately 1096 K and 137 K, respectively. The results show clearly the development of the phonon anomalies as the Fermi surface sharpens. The most conspicuous feature is the softening at $q \approx 0.76\ \pi/a$, which corresponds to the nesting vector $q = k_1 + k_3$. For large Fermi surface broadening, the dispersion curves are very similar to those of the (3, 3) pristine case [5], except that the frequencies of some branches are lower in frequency in the doped case. This is not unexpected since the excess electrons occupy the anti-bonding states, and this would typically weaken the carbon bonds [17]. The lattice dynamics is only weakly affected by electron doping at high temperatures. However, we see a lot more Kohn anomalies as the Fermi surface sharpens. In particular, the phonon becomes soft at about the same $q = 0.76\ \pi/a$ at a Gaussian width of $w = 0.025$ eV. A similar sequence of softening was also observed for the pristine (3, 3) tube as the Fermi surface sharpens [5]. In particular, at $w = 0.025$ eV, the lattice is definitively unstable for both the pristine and the doped tube. As $w = 0.025$ eV corresponds to an effective temperature of about 137 K, the T_D of both the pristine and doped tube should be above 137 K. So, at a first glance, the behavior is rather similar for doped and pristine (3, 3). However, as shown below, the softening is actually driven by different phonons coupled to different electronic states.

In figure 3, the phonon dispersion curves of six different symmetry classes for both the doped and pristine tubes are plotted for a Fermi surface smearing of $w = 0.025$ eV. The nesting q-vectors for the doped case are marked in the figure for easy visualization. The solid lines correspond to the doped tube, while the dashed lines are those for the pristine tube. For symmetry class 1 (full symmetry), we found that the pristine tube has no obvious Kohn anomalies, while the highest frequency branch for the doped tube has a Kohn anomaly corresponding to $q = k_1 + k_3$. This $q = k_1 + k_3$ is only present in the doped tube, and therefore there is no corresponding anomaly in the pristine tube. For symmetry class 2, the pristine tube has anomalies at the zone center, which is due to the nesting vector $q = k_2 - k_1 = 0$. The $q = k_2 - k_1$ anomaly for the doped tube should be found at about $q = 0.34$, and indeed we found a small dip there. The highest branch for the doped tube has a deep and broad anomaly near the zone center, which can be traced to a combination of the coupling to $k_4 - k_3$ and $k_3 - k_2$ both having magnitudes less than 0.1 π/a. Because of hybridization with the highest branch, the lowest branch is driven soft. This instability thus has its origin in interband couplings which are not present in the pristine tube. There are no observable anomalies in symmetry class 3 for either the doped or the pristine tube. For symmetry class 4, the pristine tube shows an instability at $q = 2k_1 = 2k_2$ [5]. The doped tubes show Kohn anomalies at $2k_4$ and $2k_2$. We note that for the pristine tube $k_1 = k_2$, and when excess electrons fill the band in the doped case the anomalies should split into

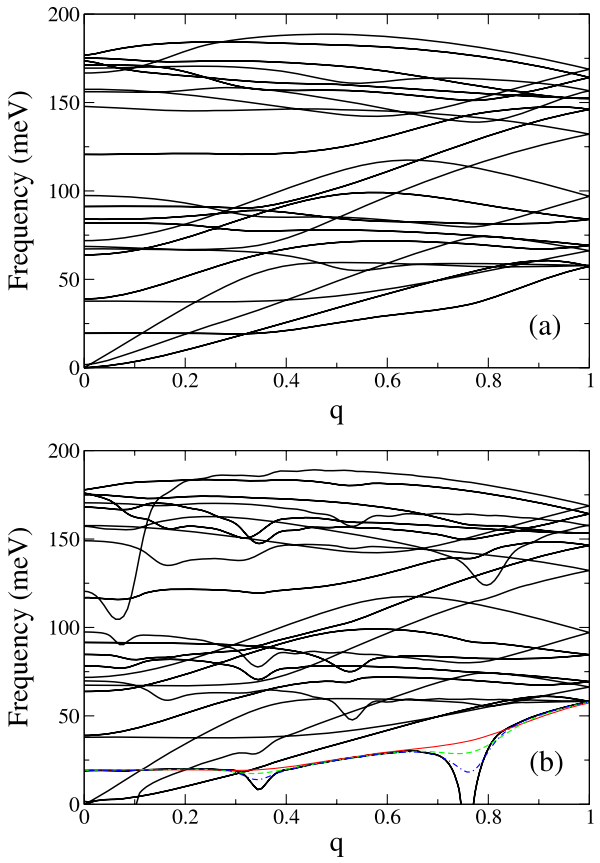

Figure 2. The phonon dispersions for the electron doped (3, 3) tube computed with Gaussian broadening widths of (a) 0.2 eV and (b) 0.025 eV. The latter one also includes the dispersion curves of the unstable phonon branch for broadenings of 0.2 eV, 0.1 eV and 0.05 eV (thin solid, dashed and dashed–dotted lines, respectively). q is given in units of π/a.

two dips, one at $q = 2k_1 \approx 0.80\ \pi/a$ for the negative mass band, and the other at $q = 2k_2 \approx 0.52\ \pi/a$ (after folding back to the irreducible BZ). We see that the anomalies due to the $q = 2k_1$ and $q = 2k_2$ nestings become much weaker. The anomaly at $q = 2k_2$ is comparatively stronger than the anomaly at $q = 2k_1$ (which is hardly visible to the eye). In addition, a new anomaly at $q = 2k_4$ appears due to the positive mass band. For symmetry class 5, the pristine tube has no discernible dips while the doped tubes have dips that can be traced to $q = k_4 - k_1$. We found the strongest phonon softening for the doped tube in symmetry class 6. In the lowest frequency branch, the phonon becomes soft near $q = k_1 + k_3$. Kohn anomalies are also found at other q vectors. There is no anomaly for the pristine tube.

Summarizing, we see that at $w = 0.025$ eV the phonons of both the pristine and the doped tube are soft, but the Peierls instabilities are driven by different nesting vectors. For the case of the pristine tube, it is a $q = 2k_1 = 2k_2$ nesting that drives the tube unstable (soft mode in symmetry class 4), but the same nesting vectors are split and become weakened in the doped tube, leading to Kohn anomalies rather than soft modes. In the doped tube, there are interband couplings (cannot be found in the pristine tube) that drive the tube to be soft (symmetry classes 2 and 6). As far as we can tell, both the pristine and the

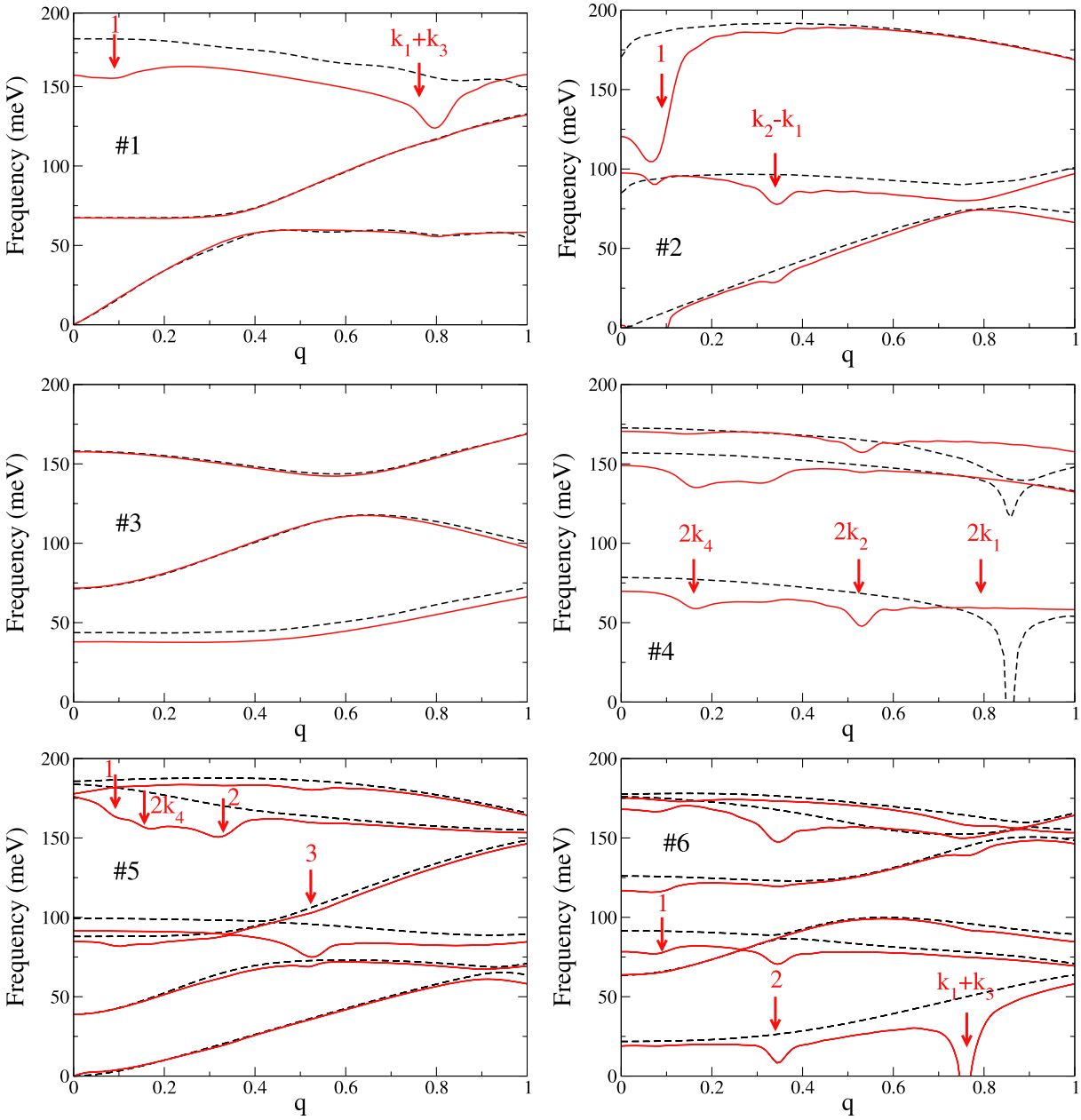

Figure 3. The phonon dispersion curves of six different symmetry classes computed with a Fermi surface smearing of $w = 0.025$ eV. The solid (dashed) lines correspond to the electron doped (pristine) tube. Nesting q-vectors are marked in some panels for easy reference. Groups of nesting vectors with similar magnitudes are denoted by 1, 2, and 3, and correspond to $(k_4 - k_3, k_3 - k_2)$, $(2k_3, k_2 - k_1, k_2 + k_4)$, and $(k_4 - k_1, 2k_2)$, respectively.

doped tube should undergo Peierls transition well above the superconducting temperature, but for a different type of el–ph coupling.

3.3. Superconductivity

The strength of the el–ph interaction can be characterized by the microscopic el–ph coupling parameters. The coupling constant for a particular phonon mode labeled by (q, α) can be written as [5]

$$\lambda_{q,\alpha} = \frac{2}{\hbar N(E_F)\omega_{q,\alpha}} \sum_{k,n,n'} |g^{q,\alpha}_{k+q,n';k,n}|^2 \delta(\epsilon_{k,n})\delta(\epsilon_{k+q,n'}), \quad (1)$$

where $N(E_F)$ is the density of states per spin at the Fermi level and n, n' are band indices. $g^{q,\alpha}_{k+q,n';k,n}$ denotes the el–ph matrix element that couples the states $|k, n\rangle$ and $|k + q, n'\rangle$ by the change in crystal lattice potential induced by the phonon mode with wavevector q and mode number α.

In the present system, only a small set of q contributes to the total el–ph coupling constant, so that we can write

$$\lambda = \frac{1}{N_q} \sum_{q,\alpha} \lambda_{q,\alpha} .$$

For the (3, 3) tube, only two q values at $q = 0$ and $q = 2k_F$ contribute. For the electron doped (3, 3) tube, there are four

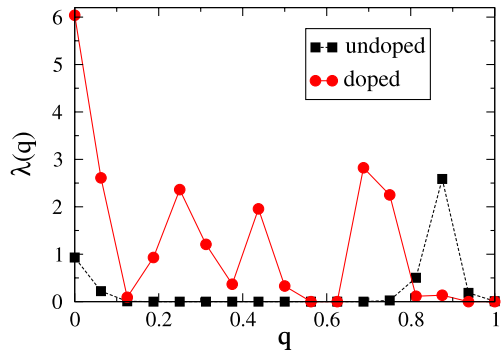

Figure 4. Comparison of $\lambda(q)$ for the pristine and the electron doped (3, 3) tube calculated with a broadening of 0.2 eV.

k-points at the Fermi level, and the corresponding set of allowed q values is listed in table 1.

Figure 4 compares the $\lambda(q) = \sum_\alpha \lambda_{q\alpha}$ for the pristine and the electron doped (3, 3) tube. Equation (1) is evaluated by replacing the δ-functions by Gaussians with a width of 0.2 eV, which leads to peaks with finite width in $\lambda(q)$. As expected, $\lambda(q)$ for the pristine tube shows only two peaks at $q = 0$ and $2k_F$, and integrates to a total value of 0.25. For the doped tube, the four possible Fermi points lead to multiple q values, and the $\lambda(q)$ function is richer in structure. The integrated $\lambda(q)$ is 1.14, which is significantly larger than the value for the pristine tube. To give a rough estimate of the superconducting transition temperature T_c, we have solved the linearized gap equations of the Eliashberg theory [18] for various values of the effective electron–electron interaction constant μ^* using the spectral function

$$\alpha^2 F(\omega) = \frac{\omega}{2N_q} \sum_{q,\alpha} \lambda_{q,\alpha} \delta(\omega - \omega_{q,\alpha}).$$

The results are shown in table 2.

We note that the calculated value of λ actually depends on the smearing of the Fermi surface (the effective temperature) since the phonon frequency enters the formula explicitly. Whenever there is phonon softening due to el–ph coupling, the phonon frequency changes with temperature and there is thus an explicit temperature dependence of λ. However, the value of the effective phonon frequency $\omega_{\ln} = \exp(1/(\lambda N_q) \sum_{q,\alpha} \lambda_{q,\alpha} \ln \omega_{q,\alpha})$ also changes at the same time. At the phonon softening temperature, λ diverges and $\omega_{\ln}$ goes to zero, but the value of T_c stays reasonably constant. In table 2, we compare the values of T_c obtained at three different effective temperatures, showing that the value of T_c remains relatively stable, even though the values of λ and $\omega_{\ln}$ change individually.

Although these values of T_c for the doped tube are qualitative, comparing them with the corresponding values of T_c for the pristine tube (computed with exactly the same procedure [5]) shows that superconductivity is indeed enhanced by electron doping. The outcome is consistent with the enhanced superconductivity behavior in graphite-intercalated compounds and alkali–C_{60} compounds.

Table 2. T_c for the electron doped tube estimated by solving the linearized gap equations of the Eliashberg theory for different values of the effective electron–electron interaction constant μ^*, with phonon frequencies and the el–ph coupling constants calculated using different Gaussian broadenings. The T_c values we obtained are quite independent of the Gaussian smearing used, as long as the lattice remains stable.

	w (eV)		
	0.05	0.1	0.2
μ^*	T_c (K)	T_c (K)	T_c (K)
0.0	64	65	69
0.04	51	51	54
0.08	41	41	43
0.10	38	37	38
0.12	35	34	35
0.14	32	30	31

4. Summary

Using density functional perturbation method, we calculated the phonon dispersion for the small diameter (3, 3) tube doped with electrons. The electron doping changes the Fermi points and thus changes the el–ph coupling significantly. The el–ph coupling drives the lattice to become unstable when the Fermi surface sharpens (or equivalently when temperature is lowered), and the Peierls transition temperature of the doped tube and the undoped tube are rather similar. However, the instability is driven by different phonons coupled to different electronic states. We estimated the superconducting temperature of the electron doped tube from the el–ph coupling matrix elements, and we found that the T_c in the electron doped tube is substantially higher than the pristine tube. In other words, the T_c for superconductivity is enhanced but the Peierls instability is not suppressed. The Peierls temperature is still higher than the superconducting T_c by a big margin. We note that superconducting behavior was observed experimentally in 0.4 nm diameter nanotubes, but all DFT calculations found that for an isolated tube the Peierls transition temperature was higher than the superconducting T_c. There are a few mechanisms that can suppress the Peierls instability, and examples are suppression of 1D characteristics due to coupling to host, tube–tube coupling [19], or electron–electron interactions [14]. This calculation shows that the intrinsic Peierls instability of the doped tube is no better and no worse than that of the pristine tube. In addition, experiments showed that a high concentration of Li can be doped into the nanotube samples [16]. So electron doping can be achieved by intercalating with Li, and this will typically increase lateral interactions. Whatever mechanism helps to suppress the Peierls instability in the clean tube will probably be further enhanced by doping, while the T_c is significantly increased. We thus think that doping these 0.4 nm tubes with electrons may be a way to increase the superconducting temperature and to make the phenomenon more robust.

Acknowledgments

Mutual visits are supported by the DAAD-HKRGC travel grant D/05/06872 (G_HK022/05-II). Research work in Hong Kong is supported by RPC06/07.SC21.

References

[1] Dresselhaus M S, Dresselhaus G and Eklund P C 1995 *Science of Fullerenes and Carbon Nanotubes* (San Diego, CA: Academic)
Saito R, Dresselhaus G and Dresselhaus M S 1998 *Physical Properties of Carbon Nanotubes* (London: Imperial College Press)
Reich S, Thomsen C and Maultzsch J 2004 *Carbon Nanotubes* (Weinheim: Wiley–VCH)
[2] Wang N, Tang Z K, Li G D and Chen J S 2000 *Nature* **408** 51
[3] Liu H J and Chan C T 2002 *Phys. Rev.* B **66** 115416
[4] Machon M, Reich S, Thomsen C, Sanchez-Portal D and Ordejon P 2002 *Phys. Rev.* B **66** 155410
[5] Bohnen K-P, Heid R, Liu H J and Chan C T 2004 *Phys. Rev. Lett.* **93** 245501
[6] Connetable D, Rignanese G-M, Charlier J-C and Blasé X 2005 *Phys. Rev. Lett.* **94** 015503
[7] Tang Z K, Zhang L, Wang N, Zhang X X, Wen G H, Li G D, Wang J N, Chan C T and Sheng P 2001 *Science* **292** 2467
[8] Benedict L X, Crespi V H, Louie S G and Cohen M L 1995 *Phys. Rev.* B **52** 14935
[9] See, e.g. Gunnarsson O 1997 *Rev. Mod. Phys.* **69** 575
[10] Liu H J and Chan C T 2003 *Solid State Commun.* **125** 77
[11] Baroni S, Giannozzi P and Testa A 1987 *Phys. Rev. Lett.* **58** 1861
[12] Meyer B, Elsässer C and Fähnle M *FORTRAN90 Program for Mixed-Basis Pseudopotential Calculations for Crystals* (Stuttgart: Max-Planck-Institut für Metallforschung) unpublished
[13] Heid R and Bohnen K-P 1999 *Phys. Rev.* B **60** R3709
[14] Barnett R, Demler E and Kaxiras E 2005 *Phys. Rev.* B **71** 035429
[15] Piscanec S, Lazzeri M, Robertson J, Ferrari A C and Mauri F 2007 *Phys. Rev.* B **75** 035427
[16] Liu H J, Li Z M, Liang Q, Tang Z K and Chan C T 2004 *Appl. Phys. Lett.* **84** 2649
[17] Chan C T, Kamitakahara W A, Ho K M and Eklund P C 1987 *Phys. Rev. Lett.* **58** 1528
[18] Bergmann G and Rainer D 1973 *Z. Phys.* **263** 59
[19] Sheng P, private communication